Patient-Specific Computational Evaluation of Stiffness Distribution in Ascending Thoracic Aortic Aneurysm

Marzio Di Giuseppe[1], Solmaz Farzaneh[2], Massimiliano Zingales[3], Salvatore Pasta[3], Stéphane Avril[2]

[1] Department of Health Promotion, Mother and Child Care, Internal Medicine and Medical Specialties, University of Palermo, 90128, Palermo, Italy
[2] Mines Saint-Etienne, Univ Lyon, Univ Jean Monnet, INSERM, U1059 SAINBIOSE, Saint-Étienne, 42023, France
[3] Department of Engineering, Viale delle Scienze, Ed.8, University of Palermo, 90128, Palermo, Italy

Submitting for Original Article

Manuscript word count: 3360 words

Corresponding author:
Stéphane Avril
Univ Lyon, INSERM U1059,
Mines Saint-Etienne, SAINBIOSE, F-42023,
158 cours Fauriel,
42023 SAINT-ETIENNE cedex 2, France
Phone: +33477420188
Fax : +33477420000
Email: avril@emse.fr

Abstract

Quantifying local aortic stiffness properties in vivo is acknowledged as essential to assess the severity of an ascending thoracic aortic aneurysm (ATAA). Recently, the LESI (local extensional stiffness identification) methodology has been established to quantify non-invasively local stiffness properties of ATAAs using electrocardiographic-gated computed tomography (ECG-gated CT) scans. The aim of the current study was to determine the most sensitive markers of local ATAA stiffness estimation with the hypothesis that direct measures of local ATAA stiffness could better detect the high-risk patients.

A cohort of 30 patients (12 BAV and 18 TAV) referred for aortic size evaluation by ECG-gated CT were recruited. For each patient, the extensional stiffness Q was evaluated by the LESI methodology whilst computational flow analyses were also performed to derive hemodynamics markers such as the wall shear stress (WSS).

A strong positive correlation was found between the extensional stiffness and the aortic pulse pressure ($R=0.644$ and $p<0.001$). Interestingly, a significant positive correlation was also found between the extensional stiffness and patients age for BAV ATAAs ($R=0.619$ and $p=0.032$), but not for TAV ATAAs ($R=-0.117$ and $p=0.645$). No significant correlation was found between the extensional stiffness and WSS evaluated locally. There was no significant difference either in the extensional stiffness between BAV ATAAs and TAV ATAAs ($Q=3.6\pm2.5$ MPa.mm for BAV ATAAs vs $Q=5.3\pm3.1$ MPa.mm for TAV ATAAs, $p=0.094$).

Future work will focus on relating the extensional stiffness to the patient-specific rupture risk of ATAAs on larger cohorts to confirm the promising interest of the LESI methodology.

Keywords: Ascending Thoracic Aortic Aneurysm, Bicuspid Aortic Valve, Extensional Stiffness, Noninvasive Inverse Method, Shear Stress

Introduction

Ascending thoracic aortic aneurysm (ATAA) is a life-threatening cardiovascular disease, leading to weakening of the aortic wall and permanent dilation. ATAA affects approximately 10 out of 100,000 persons per year in the general population (Coady et al., 1999), and this disease is associated with a high risk of mortality and morbidity (Elefteriades and Farkas, 2010). Bicuspid aortic valve (BAV) is a predisposing risk factor to ATAA formation and development with patients having associated aortopathy on approximately 40% of whole bicuspid population (Verma and Siu, 2014) and higher rate of aortic dissection compared to patients with the tricuspid aortic valve (TAV) (Januzzi et al., 2004).

To avoid aortic complications (i.e. rupture or dissection), the current clinical management of ATAA is based on strict monitoring of the aneurysm size and elective repair is recommended when aortic diameter reaches a critical size (Borger et al., 2018). However, aortic size is not a sufficient predictor of the risk of ATAA failure (Pape et al., 2007). Aortic stiffness is associated with progressive aortic dilatation and aneurysm formation as shown by imaging modalities (Longobardo et al., 2017; Teixeira et al., 2012), computational analyses (Farzaneh et al., 2019a; Martin et al., 2013a; Pasta et al., 2017a) and biomechanical studies (Selvin et al., 2010; Smoljkic et al., 2017). High aortic stiffness was associated with high rates of surgical aortic replacement and aortic root dilation in children and adults with connective tissue disorders (Prakash et al., 2015). In Marfan patients, aortic stiffness proved to be important in predicting progressive aortic dilatation (Guala et al., 2019; Sulejmani et al., 2017). A recent study of abdominal aortic aneurysms found that segmental stiffening of the aorta preceded aneurysm growth and introduced the concept that stiffening may act as an early mechanism triggering elastin breakdown and aneurysm growth (Raaz et al., 2015). Imaging based on 4D Flow MRI (Mahadevia et al., 2014), in silico computational modeling (Mendez et al., 2018; Pasta et al., 2017b) or combination of them (Youssefi et al., 2017) have confirmed an altered hemodynamic environment in BAV ATAAs with well-functioning or

stenotic aortic valve leaflets (van Ooij et al., 2017). The underlying hypothesis is that flow disturbances induce local wall shear stress (WSS) forces on the dilated aorta, portending to adverse vascular remodeling by mechanotransduction. This can further lead to changes in the biomechanical properties of ATAA wall as reflected by an increased stiffness for the dilated aorta.

Risk assessment based on the aortic stiffness of the ATAA wall are being developed (Duprey et al., 2016; Farzaneh et al., 2019b; Martin et al., 2013a). In this way, the quantification of local elastic properties of the ATAA wall from in vivo data is crucial to establish a reliable method for estimating the severity of an ATAA (Mousavi and Avril, 2017; Rooprai et al., 2019). Most importantly, new strategies of risk assessment should be accurate and compatible with clinical time framework. For that purpose, the in vivo non-invasive identification of aortic stiffness would be essential for clinicians to improve the clinical decision making process. Recently, Farzaneh et al. (Farzaneh et al., 2019a) have presented a novel methodology, namely the LESI (local extensional stiffness identification) methodology, to non-invasively quantify local stiffness properties on the basis of ECG-gated CT scans and brachial arm pressure. The interrelationship between the obtained local stiffness with other established markers of aortic function remains unclear and this currently limits the methodology's potential impact. The aim of the current study was to determine the most sensitive markers of local ATAA stiffness estimation with the hypothesis that direct measures of local ATAA stiffness could better detect the high-risk patients. First, the patterns of extensional stiffness obtained by the LESI methodology in a cohort of 30 patients with ATAAs and different aortic valve phenotypes were analyzed. Then, the association of stiffness with demographic data and computationally derived wall shear stress (WSS) was investigated.

Methods

Study Population

After internal review board approval and informed consent, 30 patients (12 BAV and 18 TAV) referred for aortic size evaluation by electrocardiographic-gated computed tomography (ECG-gated CT) were enrolled. Table 1 shows demographic data of the patient population as well as aortic diameter. For all patients, ECG-gated CT scans were performed after intravenous injection of contrast agent to improve image quality. Imaging was carried out on a GE VCT 64-channel scanner (GE Medical Systems, Milwaukee, Wisconsin), with gantry rotation velocity of 0.5 m/s and spiral pitch of 0.984. Retrospective reconstruction of images was performed to obtain images at cardiac phases corresponding to both end-diastole and end-systole at the resolution of 512 x 512 and slice thickness of 0.625 mm. Prior to imaging, diastolic and systolic blood pressures were measured by brachial sphygmomanometer for each patient.

Images Analysis

For each patient, segmentation of ECG-gated CT images was performed at both diastolic and systolic phases using Mimics v20 (Materialise, Leuven, BE). Specifically, semi-automatic threshold-based segmentation of the aortic lumen was performed to obtain a point cloud of ATAA geometries. The same smoothing factor was applied to all phases. The three-dimensional (3D) surface of the aorta was generated for each phase and exported as STL file. Then, 3D aortic surfaces reconstructed at both cardiac phases were cut by identical cross-sectional planes in Rhinoceros (Robert McNeel & Associates, Seattle, USA) to define a domain of the aorta larger than the final segment of interest. A set of nodes was defined across each reconstructed aortic geometry, with the requirement that a node represented the position of the same material point at each phase of the cardiac cycle. For this, it was essential to reconstruct a structural mesh for all phases with an identical number of elements and nodes. The Vascular Modeling Toolkit (VMTK, Orobix, Bergamo, Italy; www.vmtk.org)

(Antiga and Steinman, 2004) was employed to generate the structural mesh from STL files. The extracted data from VMTK were postprocessed in MATLAB to extract an accurate mesh using the longitudinal and circumferential metrics obtained from VMTK. A structural mesh composed of 3871 quadrilateral shell elements, 49 along the circumferential direction and 79 along the longitudinal direction, was defined on the template geometry. Each node of the structural mesh was related to assumedly the same material points for systole and diastole phases.

The LESI methodology for calculating the extensional stiffness was described by Farzaneh et al. (Farzaneh et al., 2019a). In brief, local principal strain components (ε_1 and ε_2) were deduced by computing the spatial gradients of displacements between diastolic and systolic configurations. Although the aortic tissue is globally anisotropic and nonlinear, its mechanical behavior was linearized in the range of strains induced by pressure variations between diastole and systole, and anisotropic effects were neglected in this range. The local principal stress components ($\tau_1^0 \text{ and } \tau_2^0$) were derived by finite-element analysis (FEA) performed on the ATAA diastolic geometry using average blood pressure evaluated over the cardiac cycle (Joldes et al., 2016). To obtain radii of curvature (r_1^0 and r_2^0) and their variations (Δr_2 and Δr_1) fast and efficiently, a method based on the principle of virtual work was developed, as previously introduced in Bersi et al. (Bersi et al., 2016).

Finally it was possible, for each element, to relate the extensional stiffness to the pulsed pressure ΔP such as:

$$Q = \frac{\Delta P + \frac{\tau_1^0 \Delta r_1}{(r_1^0)^2} + \frac{\tau_2^0 \Delta r_2}{(r_2^0)^2}}{\frac{\varepsilon_1 + \nu\varepsilon_2}{r_1^0} + \frac{\nu\varepsilon_1 + \varepsilon_2}{r_2^0}}$$

In the current study we used the concept of “extensional stiffness” (intensive property) which equals the material stiffness times the thickness and whose dimension is MPa.mm.

The aortic thickness could not be measured accurately due to the limited spatial resolution of CT.

Once LESI results were obtained for each patient, the average extensional stiffness was evaluated in each of the four quadrants, including the major, minor, anterior and posterior regions (Fig.1).

Computational Flow Analysis

Computational flow modeling was applied to study ATAA hemodynamics at systolic peak when the aortic valve is supposedly fully open (D'Ancona et al., 2013). For each patient, the fluid domain of ATAA geometry at end-systole was meshed with unstructured tetrahedral elements with size of 0.1 mm. The blood was assumed as a non-Newtonian incompressible fluid (density of 1060 kg/m3 and viscosity of 0.00371 Pa*s) adopting the Carreau model (Khanafer et al., 2006; Leuprecht and Perktold, 2001). The solution was obtained with FLUENT v18 (ANSYS Inc., Canonsburg, PA) using the SIMPLE algorithm for the pressure-velocity coupling and second order accurate discretization scheme. To include patient-specific hemodynamics conditions, the transaortic jet velocity evaluated by Doppler echocardiography was set as the inflow velocity condition at the aortic valve plane. For each outlet, we first computed the global vascular resistance and arterial compliance of each patient from echocardiographic measurements and clinical demographic data. Then, these parameters were used to compute the outflow boundary conditions of a three-element Windkessel model (comprising proximal resistance, compliance, and a distal resistance) coupled to each outflow branch. Boundary conditions were adjusted to match brachial artery pulse pressure.

After numerical solution, WSS values were obtained for the entire thoracic aorta, with further in-depth subanalysis in the ascending thoracic aorta by computing maxima at sinotubular junction (namely, analysis plane = AA1), proximal (AA2) and mid (AA3) ascending thoracic aorta for each quadrant (i.e., major, minor, anterior and posterior quadrants).

Statistical Analysis

The Rank Sum test was used to assess differences in the extensional stiffness between BAV ATAAs and TAV ATAAs. One-way Anova, followed by Holm-Sidak post-hoc test for all pair-wise comparisons, was used to assess differences of extensional stiffness among aortic quadrants. The association of the extensional stiffness with patient age, aortic pulse pressure, aortic diameter, WSS, aortic strain and stress was explored by Pearson's correlation. Statistical analyses were performed using SigmaPlot (Systat Software Inc., San Jose, California), with statistical significance set at $p=0.05$ in all cases. Data are shown as Mean ± SEM.

In addition, Principal Component Analysis (PCA) was performed for dimensionality reduction of all data computed for each patient. First two principal components were analyzed to assess separation of BAV ATAA versus TAV ATAA. The tolerance ellipse based on Hotelling's T2 at a significance level of 0.05 was calculated and shown in the score plots. Principal Component Analysis was performed using SPSS software (IBM SPSS Statistics v.17, New York, NY).

Results

Table 1 summarizes patient demographic data, systolic and diastolic pressures and aortic diameter. The distribution of age in BAV ATAAs differs significantly from that of TAV ATAAs patients (50.2 ± 7.5 years for BAV ATAAs vs 64.7 ± 7.8 years for TAV ATAAs, $p<0.01$), and this difference was confirmed by the analysis of the age on a different cohort of 159 patients (Agnese et al., 2019).

Fig. 2 and Fig. 3 show representative extensional stiffness and WSS maps obtained by the LESI methodology and CFD analyses for BAV ATAAs and TAV ATAAs, respectively. There was no significant difference in the extensional stiffness (Q) between BAV ATAAs and TAV ATAAs (Q=3.6±2.5 MPa.mm for BAV ATAAs vs Q=5.3±3.1 MPa.mm for TAV ATAAs,

p=0.094). Similarly, the mean values of the extensional stiffness did not significantly change among aortic quadrants (see Fig.4), although many patients had high values of the extensional stiffness in the minor and anterior quadrants of the ascending aorta.

The relationship of extensional stiffness as averaged among quadrants with the ascending aortic diameter and the aortic pulse pressure are shown in Fig.5A and Fig.5B. A strong positive correlation was found between the extensional stiffness and the aortic pulse pressure ($R=0.644$ and $p<0.001$), but was not significant between the extensional stiffness and the aortic diameter ($R=0.341$ and $p=0.065$). Interestingly, a significant positive correlation was found between extensional stiffness and patients age for BAV ATAAs ($R=0.619$ and $p=0.032$), but not for TAV ATAAs ($R=-0.117$ and $p=0.645$) as shown by Fig. 5C and Fig. 5D. Fig. 5E and Fig. 5F show the relationship of both strain and stress obtained in the circumferential direction with the average extensional stiffness. The extensional stiffness was inversely correlated with the circumferential strain ($R=-0.522$ and $p=0.00324$) and positively with the circumferential stress ($R=0.474$ and $p=0.008$). Correlation analysis of extensional stiffness with age (Fig.5C) also revealed that BAV ATAAs can be divided into two subgroups: 1) patients younger than 50 years old who had a relatively low extensional stiffness, 2) patients older than 55 years old who had a relatively high extensional stiffness. All analysis in Fig.5 were also broken down by aneurysm type, results are reported in Fig.A1.

Peak systolic WSSs were correlated to the average extensional stiffness for each ascending aortic level and aortic quadrant. The correlation analysis between extensional stiffness and WSS values evaluated at proximal ascending thoracic aorta (AA2) appears promising ($R=0.343$ and $p=0.080$ for AA2), but no significant correlation was found between stiffness and WSS evaluated locally for Major, Minor and Anterior quadrants. For the Posterior quadrant a correlation was identified although the obtained p-value was very close to the

255 threshold (p=0.05) and a low coefficient was obtained. Results are presented in Fig.6. All
256 analysis were also broken down by aneurysm type, results are reported in Fig.A2.
257
258 A PCA based on patient's age, aortic diameter, aortic pulse pressure, extensional stiffness
259 and WSS showed no separation of BAV ATAAs from TAV ATAAs (see Fig. 7). However, the
260 loading plot revealed that the most important variables responsible for differences between
261 BAV ATAAs and TAV ATAAs are the pulsed pressure and the patient's age.
262
263 **Discussion**
264 This study aimed to investigate the patterns of extensional stiffness from in vivo dynamic
265 imaging of ATAAs and to evaluate potential correlations with clinical data and blood shear
266 forces. The extensional stiffness did not show any significant difference between BAV ATAAs
267 and TAV ATAAs. This supports recent evidence and observations for which there should be
268 no distinction in the surgical management of BAV patients versus TAV patients (Agnese et
269 al., 2019). Recently, we performed equibiaxial mechanical testing on ascending aortic tissues
270 with either BAV or TAV (Di Giuseppe et al., 2019) and found no difference in the mean
271 values of the aortic tissue stiffness between BAV ATAAs and TAV ATAAs as reported here.
272 However, other groups who performed mechanical testing on ascending aortic tissues found
273 differences in the mean values of the aortic tissue stiffness between BAV patients and TAV
274 patients (Choudhury et al., 2009; Duprey et al., 2010; Okamoto et al., 2002; Pham et al.,
275 2013; Pichamuthu et al., 2013). We did not measure the extensional stiffness in non
276 aneurysmatic subjects as healthy subjects cannot undergo CT scans. However the stiffness
277 of healthy aortas was measured by a variety of other techniques in the literature and values
278 in a range between 150 kPa and 1000 kPa were reported, with ATAA exhibiting generally a
279 higher stiffness than healthy aortas (Azadani et al., 2013; Walraevens et al., 2008).
280
281 The correlation of patients' age with the extensional stiffness obtained by the LESI
282 methodology was strongly affected by the valve phenotype. For TAV patients, the

extensional stiffness did not vary with the patient age but increased with the age of BAV patients. This is likely a consequence of the significant difference in the age of BAV versus TAV patients. Indeed, TAV ATAAs were older than 50 years while most of patients with BAV were <50 years. We also found that BAV ATAAs can be divided into two subgroups: 1) patients younger than 50 years old who had a relatively low extensional stiffness, 2) patients older than 55 years old who had a relatively high extensional stiffness. Martin et al. (Martin et al., 2013b) showed that the biomechanical properties of dilated ascending aorta change between 50 and 60 years, and this could explain either the difference in the extensional stiffness of two subgroups of BAV ATAAs or the lack of correlation between the extensional stiffness and patient age for TAV ATAAs.

As expected, no significant correlation was found between extensional stiffness and shear stress for Major, Minor and Anterior quadrant, thereby suggesting there is no direct link between hemodynamics and biomechanical properties of ATAA wall. For the posterior quadrant, instead, a significant correlation was observed.

The extensional stiffness was significantly correlated with both the pulsed pressure and the circumferential strain and stress. Although these variables are directly involved in the derivation of the aortic stiffness in the LESI methodology, these significant correlations can also be interpreted with physiological principles.

Relations between the aortic stiffness and the pulsed pressure have been known for decades. Indeed, as the aorta becomes stiffer, the central pulsed pressure is higher due to the increase in the pulse wave velocity and the early return of reflected waves to the heart from following junctions (Fung, 1998). In a young and healthy aorta, the reflected wave tends to hit the aortic root during diastole, serving to increase diastolic pressure and hence improving perfusion of coronary arteries. In aged and stiffened aortas, the reflected hits the aortic root earlier, increasing the systolic pressure and decreasing the diastolic one. The amplitude of reflected waves increases as the arterial stiffness increases, further augmenting

central systolic pressure (Chirinos and Segers, 2010a, b; Fung, 1998; Laurent et al., 2005; Mackenzie et al., 2002; O'Rourke and Nichols, 2005). The effects of this supplemental load onto the aorta, which are direct expressions of the stiffness increase, should be reckoned for estimating the risk of rupture or dissection of ATAAs.

As expected, the extensional stiffness was also significantly correlated to the circumferential strain since circumferential strains are a direct expression of the aortic stiffness. Stiffening often triggers degradation and/or loss of a fraction of elastin fibers, leading to a reduction of the wall extensibility (Sokolis et al., 2012). Another consequence is also a decrease of the axial stretch of the aorta, producing an increase of the aortic arch curvature named unfolding (Redheuil et al., 2011). The degradation of protein networks in the extracellular matrix of ATAAs can be explained by the unbalance between protein synthesis by vascular cells and protein destruction by matrix metalloproteases (MMPs) (LeMaire et al., 2005). In the cohort from which this study group was extracted, we found that the expression level of MMP-9 is altered in BAV ATAAs vs TAV ATAAs (Gallo et al., 2018). The significant correlation between extensional stiffness and stress is very common for fibrous soft tissues, owing to their exponential stress-strain curve (García-Herrera et al., 2012). This reflects reorientation and straightening of collagen bundles upon loading (Sokolis et al., 2006).

When analyzing BAV and TAV ATAAs together, the PCA analysis suggested that BAV ATAAs are likely forming a cluster in the lower quadrants of the multivariate score plot in the direction of the loading associated to patient age. This is not surprising because BAV patients are known to commonly develop ATAA at younger age than TAV (Agnese et al., 2019; LeMaire et al., 2005).

Limitations

The LESI approach relies on local equilibrium equations as it is based on the principle of virtual work (Bersi et al., 2016). As for the generalized Laplace's law, the LESI approach considers the local equilibrium between pressures and tensions in a membrane, indicating that the aortic wall experience no shear through the thickness. This may not be a realistic

assumption in regions near the aortic branches but these were excluded from the analysis. The peripheral pulsed pressure rather than central aortic pressure was used. However, the mismatch of aortic compliance between the brachial artery and the aorta should be likely reduced or even reversed with the advanced age of our patients. The effect of brachial blood pressure on the extensional stiffness evaluations will be likely minimal in this study. Validation of in silico modeling has to be established. A large sample size including BAV ATAAs matched with the age of TAV ATAAs would be ideal to confirm observations. Unfortunately, we could not compare results with those relative of non aneurysmatic subjects because healthy control volunteers are not allowed to undertake multiphase gated CT scans due to x-ray radiations risks. We are trying to extend our methodology to other imaging modalities (ultrasounds, MRI).

Conclusions

We evaluated the patterns of extensional stiffness from the in vivo imaging of ATAAs on a cohort of 30 patients using the LESI methodology. We found no appreciable differences between BAV and TAV patients. Regional differences appeared marginal due to inter-individual variability. The correlation of patients' age with the extensional stiffness strongly depended on the valve phenotype. Strong relationship of the extensional stiffness with the pulsed pressure was found, supported by biomechanical explanations.

Acknowledgments

Stéphane Avril is grateful to the European Research Council (ERC grant Biolochanics, grant number 647067) for financial support. This work was supported by a "Ricerca Finalizzata" grant from the Italian Ministry of Health (GR-2011-02348129) to Salvatore Pasta, and by grant from PON FSE-FESR Ricerca Innovazione 2014–2020 to Marzio Di Giuseppe.

Conflict of interest statement

The authors confirm there are not conflict of interest associated with this publication.

Reference

Agnese, V., Pasta, S., Michelena, H.I., Minà, C., Romano, G.M., Carerj, S., Zito, C., Maalouf, J.F., Foley, T.A., Raffa, G., Clemenza, F., Pilato, M., Bellavia, D., 2019. Patterns of ascending aortic dilatation and predictors of surgical replacement of the aorta: A comparison of bicuspid and tricuspid aortic valve patients over eight years of follow-up. Journal of Molecular and Cellular Cardiology 135, 31-39.

Antiga, L., Steinman, D.A., 2004. Robust and objective decomposition and mapping of bifurcating vessels. IEEE Transactions on Medical Imaging 23, 704-713.

Azadani, A.N., Chitsaz, S., Mannion, A., Mookhoek, A., Wisneski, A., Guccione, J.M., Hope, M.D., Ge, L., Tseng, E.E., 2013. Biomechanical properties of human ascending thoracic aortic aneurysms. The Annals of Thoracic Surgery 96, 50-58.

Bersi, M.R., Bellini, C., Di Achille, P., Humphrey, J.D., Genovese, K., Avril, S., 2016. Novel methodology for characterizing regional variations in the material properties of murine aortas. Journal of Biomechanical Engineering 138, 071005.

Borger, M.A., Fedak, P.W.M., Stephens, E.H., Gleason, T.G., Girdauskas, E., Ikonomidis, J.S., Khoynezhad, A., Siu, S.C., Verma, S., Hope, M.D., Cameron, D.E., Hammer, D.F., Coselli, J.S., Moon, M.R., Sundt, T.M., Barker, A.J., Markl, M., Della Corte, A., Michelena, H.I., Elefteriades, J.A., 2018. The american association for thoracic surgery consensus guidelines on bicuspid aortic valve–related aortopathy: full online-only version. The Journal of Thoracic and Cardiovascular Surgery 156, e41-e74.

Chirinos, J.A., Segers, P., 2010a. Noninvasive evaluation of left ventricular afterload: part 1: pressure and flow measurements and basic principles of wave conduction and reflection. Hypertension 56, 555-562.

Chirinos, J.A., Segers, P., 2010b. Noninvasive evaluation of left ventricular afterload: part 2: arterial pressure-flow and pressure-volume relations in humans. Hypertension 56, 563-570.

Choudhury, N., Bouchot, O., Rouleau, L., Tremblay, D., Cartier, R., Butany, J., Mongrain, R., Leask, R.L., 2009. Local mechanical and structural properties of healthy and diseased human ascending aorta tissue. Cardiovascular Pathology 18, 83-91.

Coady, M.A., Rizzo, J.A., Goldstein, L.J., Elefteriades, J.A., 1999. Natural history, pathogenesis and etiology of thoracic aortic aneurysms and dissections. Cardiology Clinics 17, 615-635.

D'Ancona, G., Amaducci, A., Rinaudo, A., Pasta, S., Follis, F., Pilato, M., Baglini, R., 2013. Haemodynamic predictors of a penetrating atherosclerotic ulcer rupture using fluid–structure interaction analysis. Interactive Cardiovascular and Thoracic Surgery 17, 576-578.

Di Giuseppe, M., Alotta, G., Agnese, V., Bellavia, D., Raffa, G.M., Vetri, V., Zingales, M., Pasta, S., Pilato, M., 2019. Identification of circumferential regional heterogeneity of ascending thoracic aneurysmal aorta by biaxial mechanical testing. Journal of Molecular and Cellular Cardiology 130, 205-215.

Duprey, A., Khanafer, K., Schlicht, M., Avril, S., Williams, D., Berguer, R., 2010. In vitro characterisation of physiological and maximum elastic modulus of ascending thoracic aortic aneurysms using uniaxial tensile testing. European Journal of Vascular and Endovascular Surgery 39, 700-707.

Duprey, A., Trabelsi, O., Vola, M., Favre, J.-P., Avril, S., 2016. Biaxial rupture properties of ascending thoracic aortic aneurysms. Acta Biomaterialia 42, 273-285.

Elefteriades, J.A., Farkas, E.A., 2010. Thoracic aortic aneurysm: clinically pertinent controversies and uncertainties. Journal of the American College of Cardiology 55, 841-857.

Farzaneh, S., Trabelsi, O., Avril, S., 2019a. Inverse identification of local stiffness across ascending thoracic aortic aneurysms. Biomechanics and Modeling in Mechanobiology 18, 137-153.

Farzaneh, S., Trabelsi, O., Chavent, B., Avril, S., 2019b. Identifying local arterial stiffness to assess the risk of rupture of ascending thoracic aortic aneurysms. Annals of Biomedical Engineering 47, 1038-1050.

Fung, Y.-C., 1998. Biomechanics: circulation. Springer 9, 155.

Gallo, A., Agnese, V., Coronnello, C., Raffa, G.M., Bellavia, D., Conaldi, P.G., Pilato, M., Pasta, S., 2018. On the prospect of serum exosomal miRNA profiling and protein biomarkers for the diagnosis of ascending aortic dilatation in patients with bicuspid and tricuspid aortic valve. International journal of Cardiology 273, 230-236.

García-Herrera, C.M., Atienza, J., Rojo, F., Claes, E., Guinea, G., Celentano, D.J., García-Montero, C., Burgos, R., 2012. Mechanical behaviour and rupture of normal and pathological human ascending aortic wall. Medical & Biological Engineering & Computing 50, 559-566.

Guala, A., Rodriguez-Palomares, J., Dux-Santoy, L., Teixido-Tura, G., Maldonado, G., Galian, L., Huguet, M., Valente, F., Gutiérrez, L., González-Alujas, T., 2019. Influence of aortic dilation on the regional aortic stiffness of bicuspid aortic valve assessed by 4-dimensional flow cardiac magnetic resonance: comparison with Marfan syndrome and degenerative aortic aneurysm. JACC: Cardiovascular Imaging 12, 1020-1029.

Januzzi, J.L., Isselbacher, E.M., Fattori, R., Cooper, J.V., Smith, D.E., Fang, J., Eagle, K.A., Mehta, R.H., Nienaber, C.A., Pape, L.A., 2004. Characterizing the young patient with aortic dissection: results from the international registry of aortic dissection (IRAD). Journal of the American College of Cardiology 43, 665-669.

Joldes, G.R., Miller, K., Wittek, A., Doyle, B., 2016. A simple, effective and clinically applicable method to compute abdominal aortic aneurysm wall stress. Journal of the Mechanical Behavior of Biomedical Materials 58, 139-148.

Khanafer, K.M., Gadhoke, P., Berguer, R., Bull, J.L., 2006. Modeling pulsatile flow in aortic aneurysms: effect of non-Newtonian properties of blood. Biorheology 43, 661-679.

Laurent, S., Boutouyrie, P., Lacolley, P., 2005. Structural and genetic bases of arterial stiffness. Hypertension 45, 1050-1055.

LeMaire, S.A., Wang, X., Wilks, J.A., Carter, S.A., Wen, S., Won, T., Leonardelli, D., Anand, G., Conklin, L.D., Wang, X.L., 2005. Matrix metalloproteinases in ascending aortic aneurysms: Bicuspid versus trileaflet aortic valves. Journal of Surgical Research 123, 40-48.

Leuprecht, A., Perktold, K., 2001. Computer simulation of non-Newtonian effects on blood flow in large arteries. Computer Methods in Biomechanics and Biomedical Engineering 4, 149-163.

Longobardo, L., Carerj, M.L., Pizzino, G., Bitto, A., Piccione, M.C., Zucco, M., Oreto, L., Todaro, M.C., Calabrò, M.P., Squadrito, F., Di Bella, G., Oreto, G., Khandheria, B.K., Carerj, S., Zito, C., 2017. Impairment of elastic properties of the aorta in bicuspid aortic valve: relationship between biomolecular and aortic strain patterns. European Heart Journal - Cardiovascular Imaging 19, 879-887.

Mackenzie, I., Wilkinson, I., Cockcroft, J., 2002. Assessment of arterial stiffness in clinical practice. Qjm 95, 67-74.

Mahadevia, R., Barker, A.J., Schnell, S., Entezari, P., Kansal, P., Fedak, P.W., Malaisrie, S.C., McCarthy, P., Collins, J., Carr, J., 2014. Bicuspid aortic cusp fusion morphology alters aortic three-dimensional outflow patterns, wall shear stress, and expression of aortopathy. Circulation 129, 673-682.

Martin, C., Sun, W., Pham, T., Elefteriades, J., 2013a. Predictive biomechanical analysis of ascending aortic aneurysm rupture potential. Acta Biomaterialia 9, 9392-9400.

Martin, C., Sun, W., Primiano, C., McKay, R., Elefteriades, J., 2013b. Age-dependent ascending aorta mechanics assessed through multiphase CT. Annals of Biomedical Engineering 41, 2565-2574.

Mendez, V., Di Giuseppe, M., Pasta, S., 2018. Comparison of hemodynamic and structural indices of ascending thoracic aortic aneurysm as predicted by 2-way FSI, CFD rigid wall simulation and patient-specific displacement-based FEA. Computers in Biology and Medicine 100, 221-229.

Mousavi, S.J., Avril, S., 2017. Patient-specific stress analyses in the ascending thoracic aorta using a finite-element implementation of the constrained mixture theory. Biomechanics and Modeling in Mechanobiology 16, 1765-1777.

O'Rourke, M.F., Nichols, W.W., 2005. Aortic diameter, aortic stiffness, and wave reflection increase with age and isolated systolic hypertension. Hypertension 45, 652-658.

Okamoto, R.J., Wagenseil, J.E., DeLong, W.R., Peterson, S.J., Kouchoukos, N.T., Sundt, T.M., 3rd, 2002. Mechanical properties of dilated human ascending aorta. Annal of Biomedical Engineering 30, 624-635.

Pape, L.A., Tsai, T.T., Isselbacher, E.M., Oh, J.K., O'Gara P, T., Evangelista, A., Fattori, R., Meinhardt, G., Trimarchi, S., Bossone, E., Suzuki, T., Cooper, J.V., Froehlich, J.B., Nienaber, C.A., Eagle, K.A., 2007. Aortic diameter >or = 5.5 cm is not a good predictor of type A aortic dissection: observations from the International Registry of Acute Aortic Dissection (IRAD). Circulation 116, 1120-1127.

Pasta, S., Agnese, V., Di Giuseppe, M., Gentile, G., Raffa, G.M., Bellavia, D., Pilato, M., 2017a. In vivo strain analysis of dilated ascending thoracic aorta by ECG-gated CT angiographic imaging. Annals of Biomedical Engineering 45, 2911-2920.

Pasta, S., Gentile, G., Raffa, G., Bellavia, D., Chiarello, G., Liotta, R., Luca, A., Scardulla, C., Pilato, M., 2017b. In silico shear and intramural stresses are linked to aortic valve morphology in dilated ascending aorta. European Journal of Vascular and Endovascular Surgery 54, 254-263.

Pham, T., Martin, C., Elefteriades, J., Sun, W., 2013. Biomechanical characterization of ascending aortic aneurysm with concomitant bicuspid aortic valve and bovine aortic arch. Acta Biomaterialia 9, 7927-7936.

Pichamuthu, J.E., Phillippi, J.A., Cleary, D.A., Chew, D.W., Hempel, J., Vorp, D.A., Gleason, T.G., 2013. Differential tensile strength and collagen composition in ascending aortic aneurysms by aortic valve phenotype. Annals of Thoracic Surgery 96, 2147-2154.

Prakash, A., Adlakha, H., Rabideau, N., Hass, C.J., Morris, S.A., Geva, T., Gauvreau, K., Singh, M.N., Lacro, R.V., 2015. Segmental aortic stiffness in children and young adults with connective tissue disorders: relationships with age, aortic size, rate of dilation, and surgical root replacement. Circulation 132, 595-602.

Raaz, U., Zöllner, A.M., Schellinger, I.N., Toh, R., Nakagami, F., Brandt, M., Emrich, F.C., Kayama, Y., Eken, S., Adam, M., 2015. Segmental aortic stiffening contributes to experimental abdominal aortic aneurysm development. Circulation 131, 1783-1795.

Redheuil, A., Yu, W.-C., Mousseaux, E., Harouni, A.A., Kachenoura, N., Wu, C.O., Bluemke, D., Lima, J.A.C., 2011. Age-related changes in aortic arch geometry: relationship with proximal aortic function and left ventricular mass and remodeling. Journal of the American College of Cardiology 58, 1262-1270.

Rooprai, J., Boodhwani, M., Beauchesne, L., Chan, K.L., Dennie, C., Nagpal, S., Messika-Zeitoun, D., Coutinho, T., 2019. Thoracic aortic aneurysm growth in bicuspid aortic valve patients: role of aortic stiffness and pulsatile hemodynamics. Journal of the American Heart Association 8, e010885.

Selvin, E., Najjar, S.S., Cornish, T.C., Halushka, M.K., 2010. A comprehensive histopathological evaluation of vascular medial fibrosis: Insights into the pathophysiology of arterial stiffening. Atherosclerosis 208, 69-74.

Smoljkic, M., Fehervary, H., Van den Bergh, P., Jorge-Penas, A., Kluyskens, L., Dymarkowski, S., Verbrugghe, P., Meuris, B., Vander Sloten, J., Famaey, N., 2017. Biomechanical characterization of ascending aortic aneurysms. Biomechanics and Modeling in Mechanobiology 16, 705-720.

Sokolis, D.P., Kefaloyannis, E.M., Kouloukoussa, M., Marinos, E., Boudoulas, H., Karayannacos, P.E., 2006. A structural basis for the aortic stress–strain relation in uniaxial tension. Journal of Biomechanics 39, 1651-1662.

Sokolis, D.P., Kritharis, E.P., Giagini, A.T., Lampropoulos, K.M., Papadodima, S.A., Iliopoulos, D.C., 2012. Biomechanical response of ascending thoracic aortic aneurysms: association with structural remodelling. Computer Methods in Biomechanics and Biomedical Engineering 15, 231-248.

Sulejmani, F., Pokutta-Paskaleva, A., Ziganshin, B., Leshnower, B., Iannucci, G., Elefteriades, J., Sun, W., 2017. Biomechanical properties of the thoracic aorta in Marfan patients. Annals of Cardiothoracic Surgery 6, 610.

Teixeira, R., Moreira, N., Baptista, R., Barbosa, A., Martins, R., Castro, G., Providência, L., 2012. Circumferential ascending aortic strain and aortic stenosis. European Heart Journal - Cardiovascular Imaging 14, 631-641.

van Ooij, P., Markl, M., Collins, J.D., Carr, J.C., Rigsby, C., Bonow, R.O., Malaisrie, S.C., McCarthy, P.M., Fedak, P.W., Barker, A.J., 2017. Aortic valve stenosis alters expression of regional aortic wall shear

570 stress: New insights from a 4-dimensional flow magnetic resonance imaging study of 571 subjects.
571 Journal of the American Heart Association 6, e005959.
572
573 Verma, S., Siu, S.C., 2014. Aortic dilatation in patients with bicuspid aortic valve. New England Journal
574 of Medicine 370, 1920-1929.
575
576 Walraevens, J., Willaert, B., De Win, G., Ranftl, A., De Schutter, J., Vander Sloten, J., 2008. Correlation
577 between compression, tensile and tearing tests on healthy and calcified aortic tissues. Medical
578 Engineering & Physics 30, 1098-1104.
579 Youssefi, P., Gomez, A., He, T., Anderson, L., Bunce, N., Sharma, R., Figueroa, C.A., Jahangiri, M.,
580 2017. Patient-specific computational fluid dynamics—assessment of aortic hemodynamics in a
581 spectrum of aortic valve pathologies. The Journal of Thoracic and Cardiovascular Surgery 153, 8-20.
582 e23.

583

Figure 1

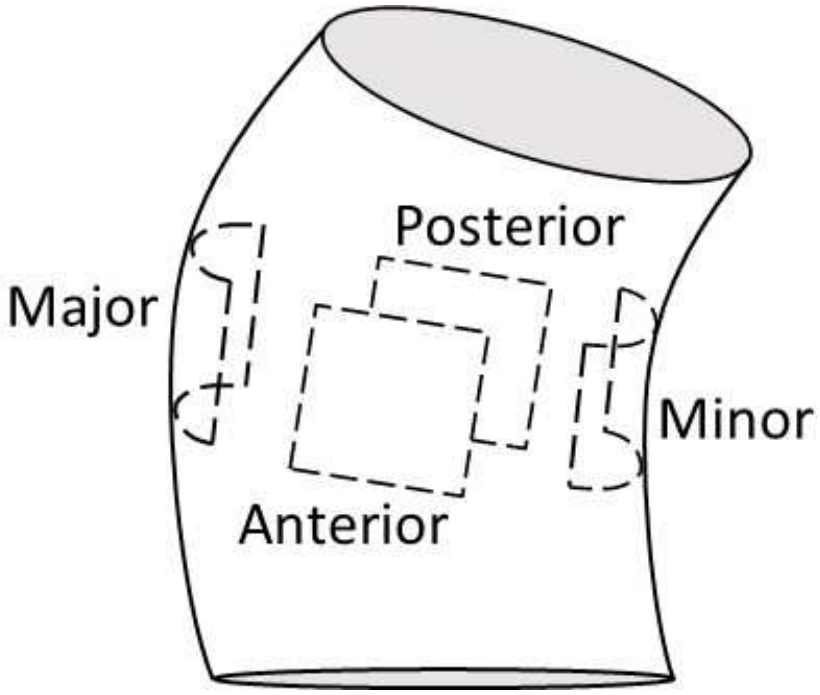

Figure 2

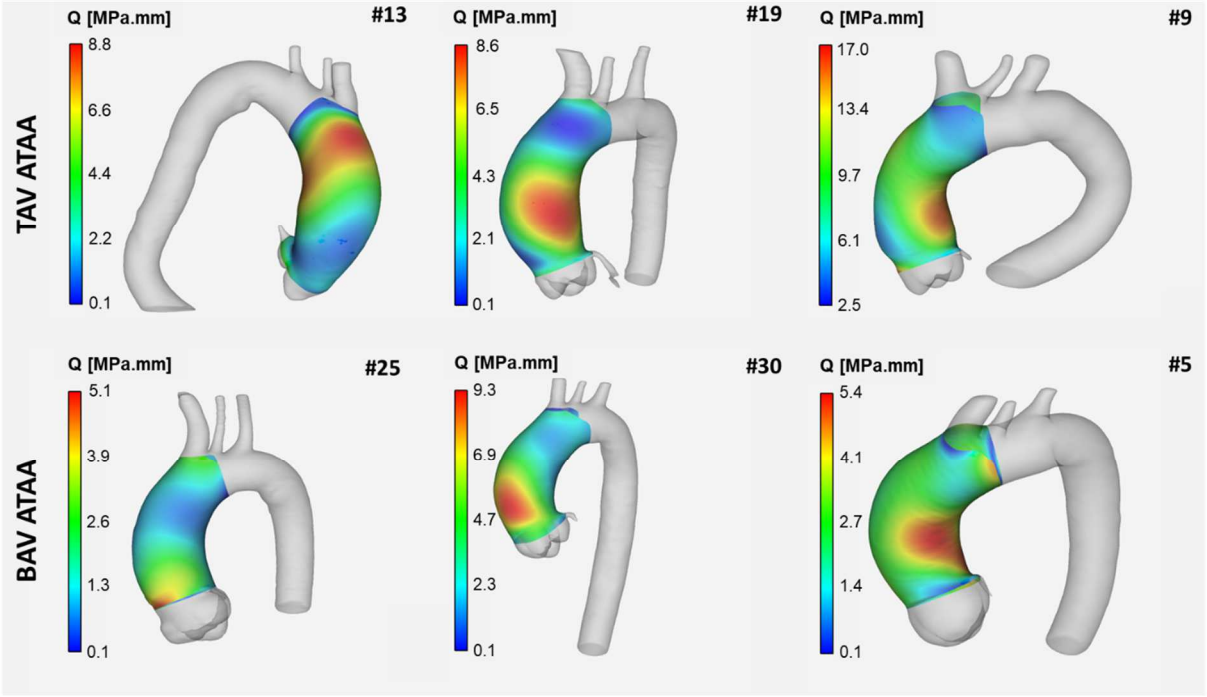
TAV ATAA
BAV ATAA
Q [MPa.mm]
8.8
6.6
4.4
2.2
0.1
#13
Q [MPa.mm]
8.6
6.5
4.3
2.1
0.1
#19
Q [MPa.mm]
17.0
13.4
9.7
6.1
2.5
#9
Q [MPa.mm]
5.1
3.9
2.6
1.3
0.1
#25
Q [MPa.mm]
9.3
6.9
4.7
2.3
0.1
#30
Q [MPa.mm]
5.4
4.1
2.7
1.4
0.1
#5

Figure 3

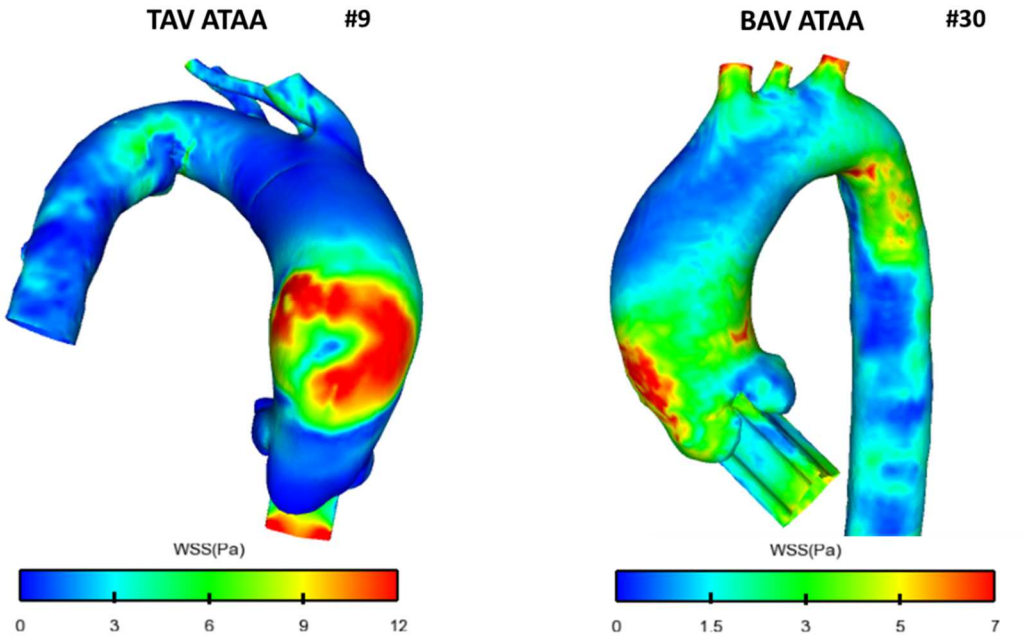

Figure 4

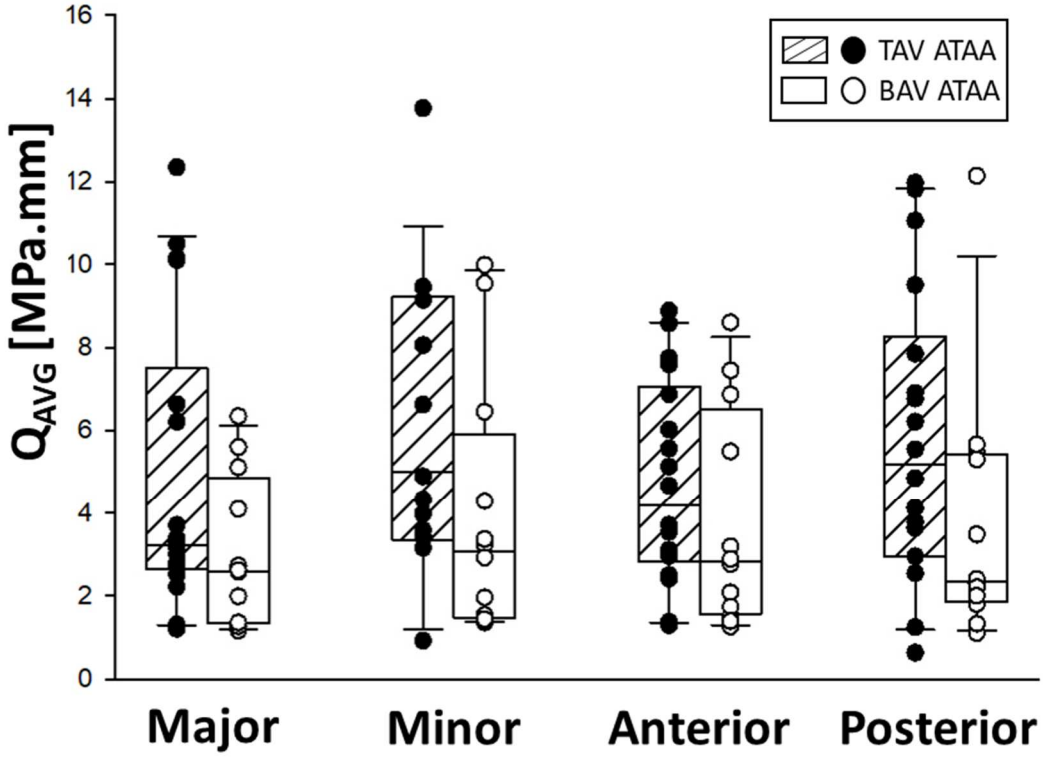
TAV ATAA
BAV ATAA
Q_{AVG} [MPa.mm]
16
14
12
10
8
6
4
2
0
Major
Minor
Anterior
Posterior

Figure 5

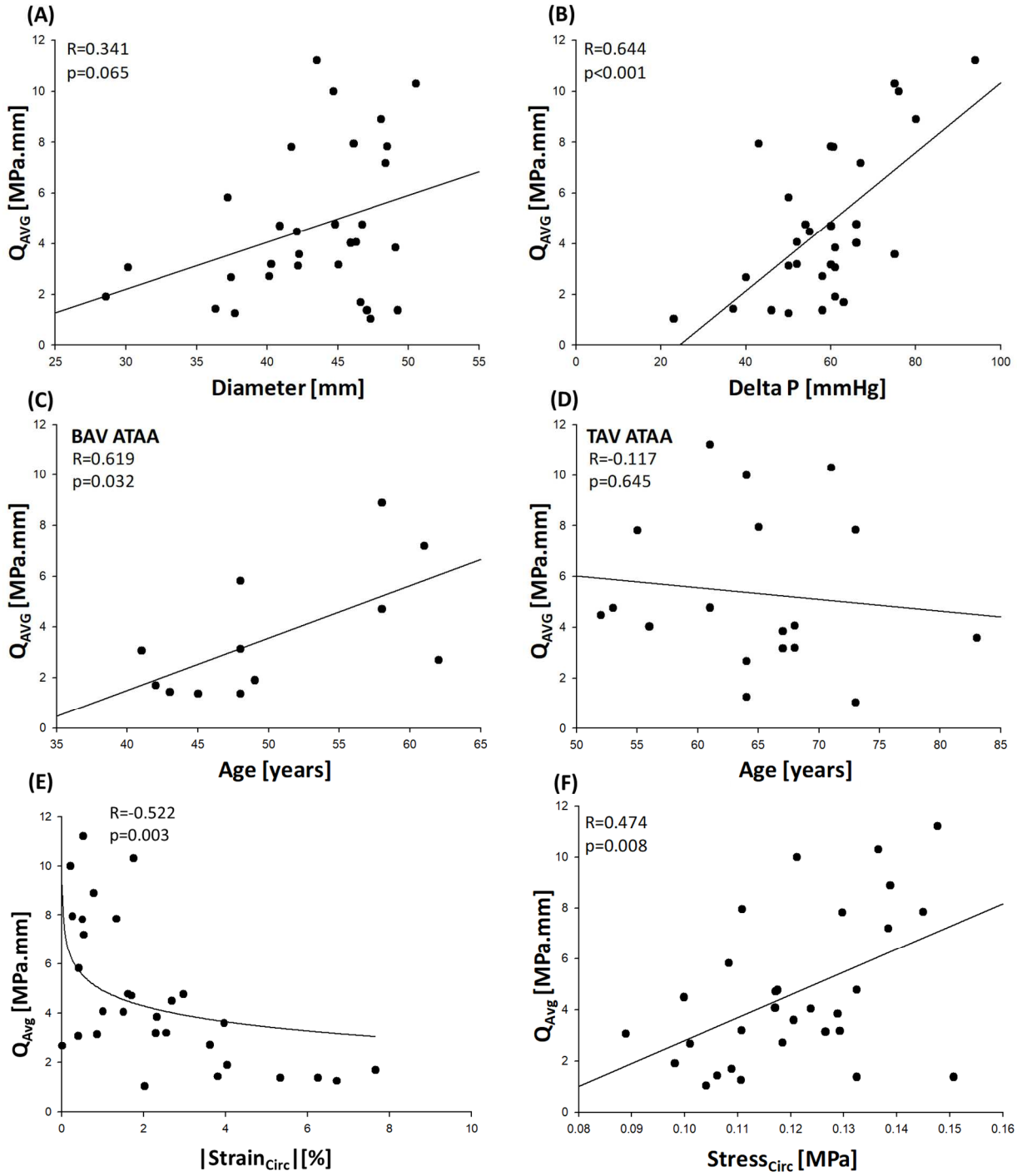
(A)
R=0.341
p=0.065
Q_{AVG} [MPa.mm]
Diameter [mm]
(B)
R=0.644
p<0.001
Q_{AVG} [MPa.mm]
Delta P [mmHg]
(C)
BAV ATAA
R=0.619
p=0.032
Q_{AVG} [MPa.mm]
Age [years]
(D)
TAV ATAA
R=-0.117
p=0.645
Q_{AVG} [MPa.mm]
Age [years]
(E)
R=-0.522
p=0.003
Q_{Avg} [MPa.mm]
$|Strain_{Circ}|$ [%]
(F)
R=0.474
p=0.008
Q_{Avg} [MPa.mm]
$Stress_{Circ}$ [MPa]

Figure 6

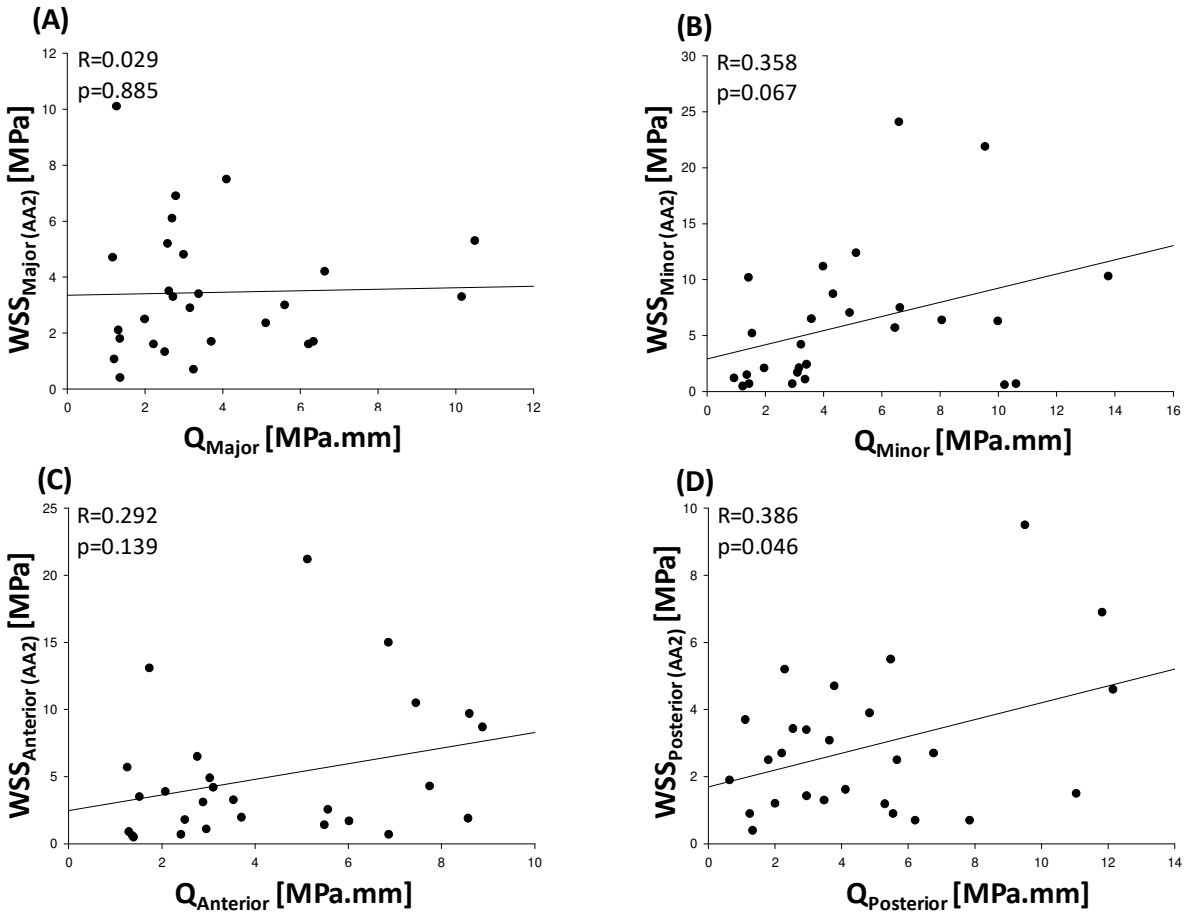
(A)
R=0.029
p=0.885
WSS Major (AA2) [MPa]
Q Major [MPa.mm]
(B)
R=0.358
p=0.067
WSS Minor (AA2) [MPa]
Q Minor [MPa.mm]
(C)
R=0.292
p=0.139
WSS Anterior (AA2) [MPa]
Q Anterior [MPa.mm]
(D)
R=0.386
p=0.046
WSS Posterior (AA2) [MPa]
Q Posterior [MPa.mm]

Figure 7

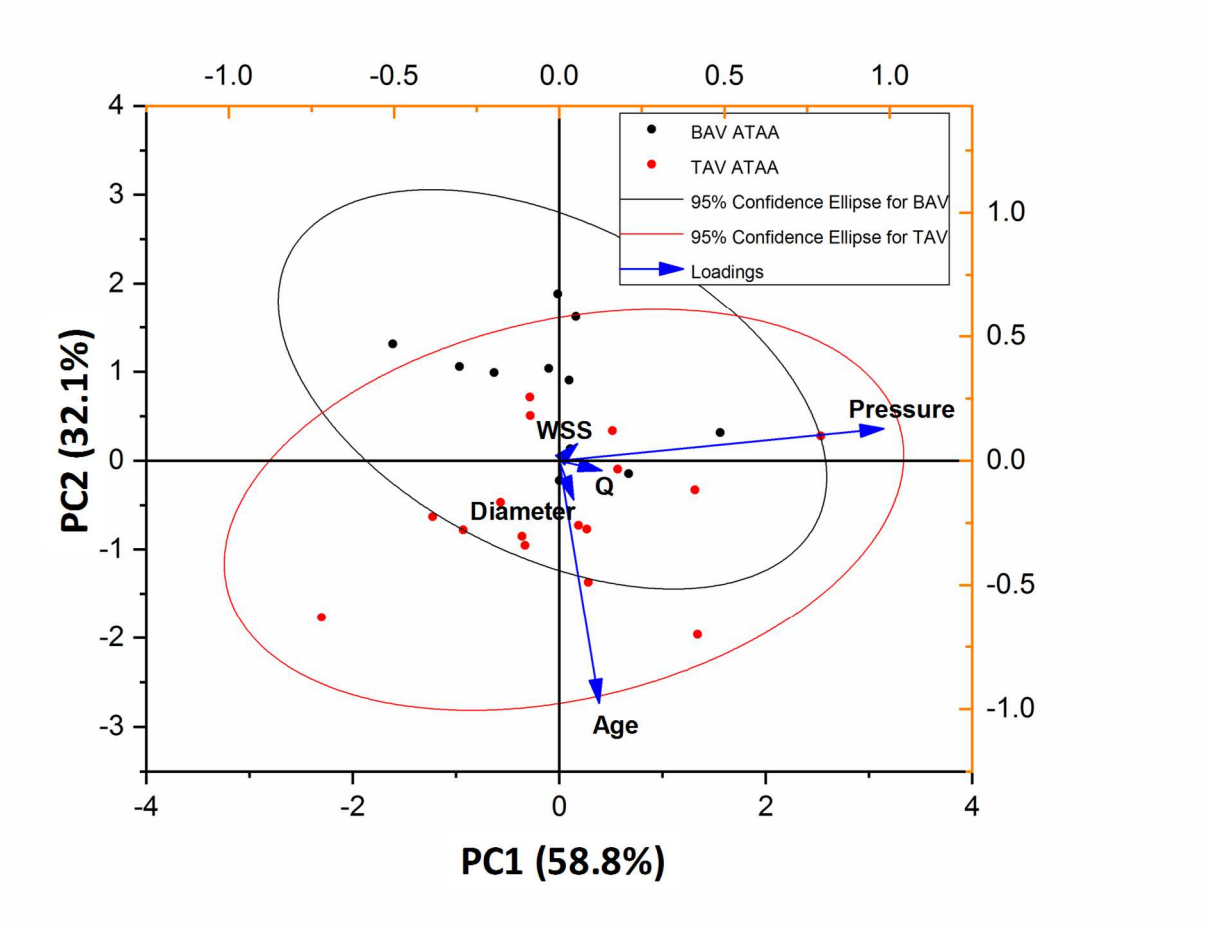
BAV ATAA
TAV ATAA
95% Confidence Ellipse for BAV
95% Confidence Ellipse for TAV
Loadings
Pressure
WSS
Q
Diameter
Age
PC1 (58.8%)
PC2 (32.1%)
-1.0
-0.5
0.0
0.5
1.0
4
3
2
1
0
-1
-2
-3
-4
-2
0
2
4
1.0
0.5
0.0
-0.5
-1.0

Table 1: Demographic and clinical data.

ID	Sex	Valve	Age [years]	Systolic Pressure [mmHg]	Diastolic Pressure [mmHg]	Aortic Diameter [mm]
1	M	TAV	56	140	74	45.9
2	M	TAV	55	136	76	41.7
3	M	BAV	62	135	77	40.13
4	M	BAV	43	125	88	36.32
5	M	BAV	48	135	85	42.15
6	M	TAV	71	145	70	50.5
7	M	BAV	58	150	70	48.04
8	M	TAV	73	100	77	47.3
9	M	TAV	61	180	86	43.5
10	M	TAV	67	136	75	49.05
11	M	TAV	67	140	80	45.01
12	M	TAV	68	122	70	46.27
13	F	TAV	83	150	75	42.23
14	M	TAV	65	116	73	46.1
15	M	TAV	61	136	70	44.8
16	M	BAV	48	130	80	37.2
17	M	BAV	49	136	75	28.56
18	M	TAV	68	129	77	40.27
19	M	TAV	53	126	72	46.7
20	F	TAV	64	144	68	44.67
21	M	TAV	73	144	84	48.47
22	M	BAV	41	136	75	30.13
23	M	BAV	42	131	68	46.59
24	M	TAV	64	120	80	37.43
25	M	BAV	48	148	90	47.05
26	M	TAV	64	130	80	37.71
27	M	BAV	45	124	78	49.21
28	F	BAV	61	144	77	48.36
29	F	TAV	52	125	70	42.1
30	M	BAV	58	136	76	40.86
			58.9±10.4	135.0±13.8	76.5±5.8	43.1±5.4